CrossMark

JM PAPERS

On the compound sessile drops: configuration boundaries and transitions

Chun-Yu Zhang[1], Peng Gao[1], Er-Qiang Li[1] and Hang Ding[1],†

[1]Department of Modern Mechanics, University of Science and Technology of China, Hefei 230027, PR China

The geometry of compound sessile drops at equilibrium on a flat substrate can exhibit a variety of complicated morphological configurations. In this paper, we first investigate the configuration boundaries of the compound sessile drops in a wide parameter space, where a specific configuration is not stable outside its boundaries. Then, we focus on the transitions among the axisymmetric configurations, i.e. encapsulation, lens and collars. The configuration transitions result from the variation of the wettability of the substrate and the volume ratio of the two component droplets. With the help of theoretical analysis and numerical simulations, we obtain previously unidentified criteria for the onset of configuration transition, identify the irreversible and reversible configuration transitions, reveal the dynamic behaviours of configuration transitions that are not accessible to theoretical analysis, and provide a further step towards the ultimate purpose of such work, which is the controllable reconfiguration of the compound sessile drops.

Key words: drops, capillary flows

1. Introduction

Compound sessile drops have gained considerable attention due to their potential uses in pharmaceutical formulations (Zarzar *et al.* 2015), drug delivery (Sundararajan *et al.* 2017) and inkjet printing (Keller *et al.* 2018). Here, the compound sessile drops refer to the drops comprised of two or more immiscible fluids and sticking to a plate substrate. The geometry of compound sessile drops at equilibrium is of great importance in industrial applications, and can exhibit a variety of complicated morphological configurations. The multiphase system involving ternary fluids in contact with a solid in figure 1 shows a good example, and it is also the focus of present paper. In this system, a compound sessile drop consisting of two fluids is immersed in a third, mutually immiscible liquid, and the morphological configurations include encapsulation, lens, collars and Janus, to name but a few. They are

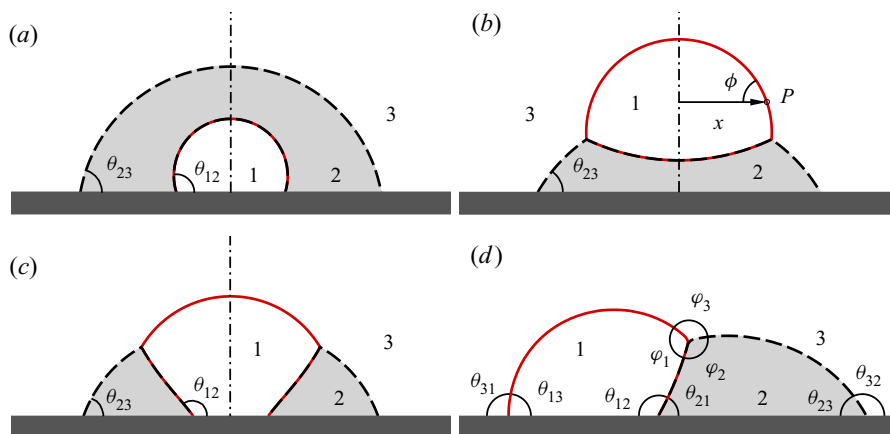† Email address for correspondence: hding@ustc.edu.cn

Figure 1. Morphological configurations of compound sessile drops resting on a flat substrate: (*a*) encapsulation, (*b*) lens, (*c*) collars and (*d*) Janus, which are also referred thereafter to as configurations *E*, *L*, *C* and *J*, respectively. Solid lines represent the surface of the component droplet 1 (made up of fluid 1), while dashed lines represent the surface of the component droplet 2 (made up of fluid 2).

distinguishable by the relative position of the component droplets of the compound drop and whether the component droplets are in contact with the substrate.

For each configuration, the geometry of the compound sessile drop at the equilibrium state is generally dictated by the minimization of the system energy, or more precisely, is related to the physical parameters including interfacial tensions, wettability of the substrate, volume of the compound drop, volume ratio of the two component droplets and gravity. Based on the Young–Laplace equation, Mahadevan, Assa-bedia & Pomeau (2002) provided the analytical expression of geometrical relations in the absence of gravity for two configurations of compound sessile drops, i.e. encapsulation and lens. Neeson *et al.* (2012) presented a theoretical description of the drop geometry in the collars configuration, for compound sessile drops with negligible gravitational effect. Furthermore, their theoretical prediction of the drop shape at equilibrium in the collars configuration was found to agree well with that in experiments, in particular when the compound sessile drops are significantly below the capillary length. Li *et al.* (2020*a*) theoretically investigated the equilibrium shape of a pendent compound droplet in the lens configuration, on which the gravitational force plays an important role. On the other hand, it is noteworthy that given the physical parameters for a compound sessile drop, its geometry at equilibrium cannot be uniquely determined. This is mainly due to the fact that multiple configurations could be stable for the same fluid parameters. Therefore, the configuration of a compound sessile drop depends on the way of generating it.

It has been reported in experiments that the transition between the morphological configurations might occur when the fluid parameters were changed. Neeson *et al.* (2012) found that if one component of a compound sessile drop can evaporate, the resulting change of the volume ratio can lead to the configuration transition, e.g. from Janus to collars or from lens to collars. Iqbal *et al.* (2017) further studied the suspension of small oil droplets at the top of the water droplets for a variety of volume ratios between the oil and water droplets, and observed that there exists a critical volume ratio, above which the lens configuration would transit to Janus. Bansal & Sen (2017) actuated the oscillations of concentric compound drops of water surrounded by an oil shell using electrowetting, which promotes the configuration transition from encapsulation to collars. To assess the

onset of configuration transition from the theoretical point of view, Mahadevan *et al.* (2002) presented a geometrical criterion, i.e. the merging of four phases along a single contact line in the encapsulation configuration, which would lead to the configuration transition from encapsulation to lens. These findings suggest the potential of controlling the configuration transition and reconfiguring the compound sessile drops in industrial applications. However, it needs systematic studies to identify all the critical conditions for the configuration transition to occur, and to determine the configuration and geometry of the compound sessile drops at equilibrium after the configuration transition takes place.

In this paper, we investigate the configuration transitions of compound sessile drops by theoretical analysis and numerical simulations, in particular among the axisymmetric configurations, i.e. encapsulation, lens and collars. In the present study, we do not consider the effect of gravity, as the size of the drops considered is much smaller than the capillary length. Here, the capillary length for the ternary fluids is defined as $l_c = \min\{\sqrt{\sigma_{ij}/|\rho_i - \rho_j|g}\}$, where ρ_i and ρ_j are the density of the fluid i and fluid j, respectively, g the gravity, σ_{ij} the interface tension coefficient between the fluid i and fluid j, the subscripts $\{i, j\} = \{1, 2, 3\}$ and $i \neq j$. The substrate is assumed to be very smooth and chemically homogeneous, and thus the effect of contact angle hysteresis is also neglected. The configuration transitions are caused by varying the wettability of the substrate (specifically θ_{23}, which exists in all the configurations, see figure 1d) and the volume ratio of the two component droplets (λ), in the range of $\lambda \in [0, 1]$ and $\theta_{23} \in [55°, 125°]$. The geometry of the compound sessile drop at equilibrium in the respective configurations is obtained by solving the related interface equations derived from the Young–Laplace equation. Here, the initial state is very important in solving the interface equations, since different final states could be reached from different initial states. A ternary-fluid diffuse-interface method is used to simulate the dynamics of configuration transition, and to examine the eventual configuration and geometry of the drop. The theoretical analysis allows us to evaluate the criteria for the onset of configuration transition, establish the boundaries in the parameter space within which the respective configuration can hold, and identify the irreversible and reversible configuration transitions. In particular, we find that the geometrical criteria are not sufficient to describe the configuration transitions. With the help of numerical simulations, we reveal the dynamic behaviours of configuration transitions that are not accessible to theoretical analysis, and assess the theoretical prediction of the drop geometry at equilibrium after the occurrence of configuration transition. Furthermore, we discuss the feasibility in the controllable reconfiguration of the compound sessile drops, and also provide a theoretical way of how to achieve this ultimate purpose.

2. Problem statement and methodology

2.1. *Problem statement*

We investigate here the configuration transition of compound sessile drops on a flat substrate, in which the compound sessile drop consists of two immiscible fluids, immersed in a third one. We mainly concentrate on the axisymmetric configurations of the compound sessile drop, including encapsulation, lens and collars, namely configurations E, L and C, respectively; a sketch of these configurations can be seen in figure 1(a–c). These configurations of compound sessile drops are primarily defined according to the relative position of its component droplets and whether the component droplets are in contact with the substrate. In the encapsulation configuration, the droplet of fluid 1 (namely droplet 1) is wrapped by the droplet of fluid 2 (namely droplet 2) in an axisymmetric manner, and

both droplets are in contact with the substrate (figure 1a). In the lens configuration, droplet 1 floats on the top of droplet 2 that is in contact with the solid substrate (figure 1b). In the collars configuration, droplet 1 is partially immersed in droplet 2, and both droplets are in contact with the substrate (figure 1c). In each configuration, the relative significance of droplet volume can be measured by the volume ratio of droplet 1 to the compound drop, λ, and thus the volume ratio of droplet 2 is $1 - \lambda$. It is noteworthy that the positions of fluid 1 and fluid 2 can be swapped in the configurations listed in figure 1(a–c).

The compound sessile drops considered are supposed to be sufficiently small so that the gravitational force can be neglected. Therefore, the force balance between the interface tensions among the fluids and the substrate dictates the shape of the compound drop at equilibrium. The interface tension coefficients between the fluids are assumed to satisfy the triangular inequality, $\sigma_{ij} < \sigma_{jk} + \sigma_{ki}$, for all cyclic permutations of the indices $\{i, j, k\} = \{1, 2, 3\}$. In such a case, the relative significance of the interface tensions between the fluids can be represented by the interfacial angles (φ_1, φ_2 and φ_3 in figure 1(d), and $\varphi_1 + \varphi_2 + \varphi_3 = 360°$) at the triple-phase line where the ternary fluids meet. Specifically, they are associated with the interface tensions by Neumann's triangle (Mahadevan *et al.* 2002),

$$\frac{\sin \varphi_1}{\sigma_{23}} = \frac{\sin \varphi_2}{\sigma_{31}} = \frac{\sin \varphi_3}{\sigma_{12}}. \tag{2.1}$$

For a compound sessile drop at equilibrium, Young's equation suggests $\sigma_{ij} \cos \theta_{ij} = \sigma_{js} - \sigma_{is}$, where σ_{js} (σ_{is}) denotes the interface tension between the fluid j (i) and the substrate. The static contact angle θ_{ij} corresponds to the angle that the interface between fluids i and j intersects with the substrate, particularly measured from the side of fluid i – geometrically, $\theta_{ij} + \theta_{ji} = 180°$ (see figure 1d). Combining Young's equation with Neumann's triangle, we can get that the interfacial angles and the contact angles should yield the following constraint (Zhang *et al.* 2016):

$$\sin \varphi_2 \cos \theta_{13} - \sin \varphi_3 \cos \theta_{12} - \sin \varphi_1 \cos \theta_{23} = 0. \tag{2.2}$$

From the analysis above, we can see that the geometry of the compound sessile drop with specific configuration can be uniquely determined, given the volume ratio λ, the interfacial angles (φ_1, φ_2 and φ_3) and any two contact angles in (2.2). The interface tension coefficients are fixed for the convenience of analysis, more specifically, $\sigma_{12} : \sigma_{23} : \sigma_{31} = 1 : \sqrt{3} : 2$, which corresponds to the interfacial angles of $\varphi_1 = 120°$, $\varphi_2 = 90°$ and $\varphi_3 = 150°$. Similarly, we set $\sigma_{1s} = \sigma_{3s}$, leading to $\theta_{13} = 90°$. Thus, it is easy to obtain from (2.2) that

$$\cos \theta_{12} = -\frac{\sigma_{23}}{\sigma_{12}} \cos \theta_{23} = -\sqrt{3} \cos \theta_{23}. \tag{2.3}$$

Note that the contact angle θ_{12} is allowed to vary from $0°$ to $180°$. Consequently, the range of θ_{23} is restricted to $[55°, 125°]$. Consequently, for a specific compound drop, the configuration of the compound sessile drop at equilibrium depends only on λ and θ_{23}.

2.2. *Theoretical prediction of drop geometry*

In this section, we present the governing equations and boundary conditions for the theoretical prediction of the geometry of the compound sessile drop. For a compound sessile drop at equilibrium, there is a force balance between Laplace excess pressure and

surface tension across any of its interface, which yields

$$p_i - p_j = \sigma_{ij}\left(\frac{1}{R_1} + \frac{1}{R_2}\right), \tag{2.4}$$

where p_i and p_j denote the constant pressure of the fluids i and j, respectively, and R_1 and R_2 represent the two principal radii of interface curvature.

The interfaces of the compound drop are described in a curvilinear coordinate (x, ϕ), where x is the distance from any point on the interface to the symmetry axis, and ϕ is the angle between the interface tangent and the horizontal direction (figure 1b). As a result, the principal radii of curvature can be represented in terms of x and ϕ,

$$R_1 = \frac{1}{\cos\phi}\frac{dx}{d\phi} \quad \text{and} \quad R_2 = \frac{x}{\sin\phi}. \tag{2.5a,b}$$

Substituting (2.5a,b) into (2.4) and defining the interface curvature as $M = (p_i - p_j)/\sigma_{ij}$, we can obtain $M = \cos\phi \cdot d\phi/dx + \sin\phi/x$. Integration of this equation over any interface that separates two fluids gives (Carroll 1976)

$$x\sin\phi = \tfrac{1}{2}Mx^2 + N, \tag{2.6}$$

where N is an integration constant associated with M and the boundaries of the interface.

Equation (2.6) provides a description of interface shapes in the coordinate (x, ϕ). To determine the shape of the compound sessile drop at equilibrium, the boundary conditions of the interfaces, i.e. the starting point (x_s, ϕ_s) and the end point (x_e, ϕ_e), and the interface parameters M and N should be explicitly obtained for every interface of compound sessile drops. In principle, these parameters are a function of λ, interface angles and contact angles, and can be determined by taking account of the geometrical and physical constraints, such as the drop volume and the force balance. Once these parameters are obtained, the rescaled surface energy of the compound sessile drop, E_S, can be calculated – see more details in the Appendix A.

The solutions of the interfaces for compound sessile drops are obtained by using a shooting method and a binary searching method. Because of the presence of the triple-phase line in the latter, the governing equations of the three interfaces are strongly coupled, and are thus solved simultaneously. For the spherical interfaces, the analytical solution of the interface can be obtained and explicitly expressed in terms of x and ϕ. However, for the non-spherical interfaces, one additional constraint is required to determine the interface shape. In this case, the interface geometry can only be obtained numerically.

2.3. *Ternary-fluid diffuse-interface model*

A ternary-fluid diffuse-interface model is coupled with Navier–Stokes equations (Zhang *et al.* 2016), to simulate the dynamic process of configuration transition of a compound sessile drop on a flat substrate. The total volume of the compound drop is denoted by V_0, which also gives rise to a characteristic length $R = \sqrt[3]{0.75V_0/\pi}$. The ternary fluids are assumed to have the same viscosity μ and density ρ. To compare with the theoretical prediction, the transition is ideally quasi-static in the numerical simulation. That is, viscosity is dominant over the inertia and surface tension of the compound sessile drop, so as to suppress the capillary waves induced by configuration transition. Therefore, it is appropriate to use a large Ohnesorge number ($Oh = \mu/\sqrt{\rho R\sigma_{13}}$), and $Oh = 0.1$ is considered to be sufficiently large for this purpose. Numerical results can be very helpful
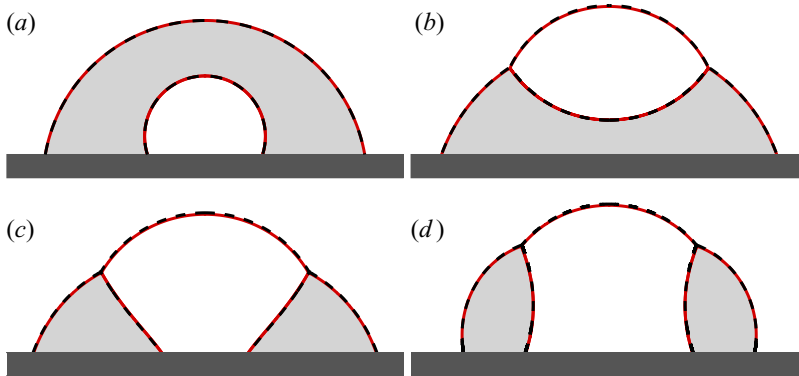
Figure 2. Verification of theoretical predictions of compound sessile drops at equilibrium. (*a*) Configuration *E* with $\lambda = 0.100$ and $\theta_{23} = 70°$. (*b*) Configuration *L* with $\lambda = 0.250$ and $\theta_{23} = 80°$. (*c*) Configuration *C* with $\lambda = 0.400$ and $\theta_{23} = 70°$. (*d*) Configuration *C* with $\lambda = 0.400$ and $\theta_{23} = 100°$. Solid lines are the numerical results and dashed lines are the theoretical prediction.

in determining whether the theoretical analysis produces physically meaningful solutions. Unless otherwise stated, all the times of numerical results have been rescaled by the capillary time $\sqrt{\rho R^3 / \sigma_{13}}$.

In the ternary-fluid diffuse-interface model, the interfaces are represented by the contours of the volume fractions of the fluids 1 and 2, i.e. C_1 and C_2, respectively. The interface evolution can be tracked by

$$\frac{\partial \mathbf{C}}{\partial t} + \nabla \cdot (\boldsymbol{u} C) = \frac{1}{Pe} \nabla^2 \boldsymbol{\Psi}, \tag{2.7}$$

where $\mathbf{C} = (C_1, C_2)$ and $\mathbf{u}$ is the flow velocity. The chemical potential $\boldsymbol{\Psi} = (\Psi_1, \Psi_2)$ is defined as

$$\Psi_i = C_i^3 - 1.5 C_i^2 + 0.5 C_i - C_1 C_2 (1 - C_1 - C_2) - Cn^2 \nabla^2 C_i, \quad i = 1 \text{ or } 2, \tag{2.8}$$

where the Cahn number is set to $Cn = 0.7h/R$, the Péclet number is set to $Pe = 1/Cn$ (Liu & Ding 2015) and h is the mesh size. More details in the numerical implementation can be found in Zhang *et al.* (2016).

Axisymmetric simulations are performed in a domain of $3R \times 2R$ on a uniform Cartesian grid of 600×400, i.e. $h = 0.005R$. The boundary conditions are: symmetry condition at the left boundary; solid wall condition at the bottom boundary; and extrapolation condition at the upper and right boundaries. The same code was used to obtain the equilibrium states of two-dimensional Janus drops on a flat substrate and a compound droplet inside a capillary (Zhang *et al.* 2016), and good agreement with the theoretical prediction of drop geometries has been achieved. In the present study, numerical simulations are also used to verify the theoretical prediction of the configurations *E*, *L* and *C*, since the theoretical prediction could lead to non-physical solutions (see more details in § 3.1). For the physical solutions, the theoretical prediction is expected to be virtually overlapped with the numerical results, with respect to the shape of compound sessile drops at equilibrium. Examples are shown in figure 2, with different volume ratio λ and contact angles θ_{23}.

917 A37-6

3. Phase diagram of compound sessile drops

We present here the phase diagram of the compound drop configurations in the parameter space of $\lambda \in [0, 1]$ and $\theta_{23} \in [55°, 125°]$. The solutions are obtained by theoretical analysis, consisting of encapsulation (§ 3.2), lens (§ 3.3) and collars (§ 3.1). For simplicity, the interface between the fluids j and k is referred to as I_{jk}, and accordingly, the geometry parameters for I_{jk} in (2.6) are denoted by (M_i, N_i), with cyclic permutations of the indices $\{i, j, k\} = \{1, 2, 3\}$.

3.1. *Collars*

A compound sessile drop with configuration C consists of three interfaces as shown in figure 3(a), among which the boundary conditions of I_{23} and I_{13} are: $\phi|_{x=r_1} = \theta_{23}$ and $\phi|_{x=r_2} = \varphi_3 + \alpha - 180°$ for I_{23}; and $\phi|_{x=r_2} = \alpha$ and $\phi|_{x=0} = 0$ for I_{13}. For I_{12}, the boundary conditions are $\phi|_{x=r_3} = \theta_{12}$ and $\phi|_{x=r_2} = 180° - \varphi_1 + \alpha$, where r_3 is the radius of contact line of droplet 1. With these boundary conditions, we can get the interface parameters

$$
\left.
\begin{aligned}
M_1 &= \frac{2(r_1 \sin \theta_{23} + r_2 \sin(\varphi_3 + \alpha))}{r_1^2 - r_2^2}, \\
N_1 &= \frac{-r_1 r_2 (r_1 \sin(\varphi_3 + \alpha) + r_2 \sin \theta_{23})}{r_1^2 - r_2^2},
\end{aligned}
\right\}
\tag{3.1}
$$

$$
\left.
\begin{aligned}
M_2 &= \frac{2 \sin \alpha}{r_2}, \\
N_2 &= 0
\end{aligned}
\right\}
\tag{3.2}
$$

and

$$
\left.
\begin{aligned}
M_3 &= \frac{2(r_3 \sin \theta_{12} - r_2 \sin(\varphi_1 - \alpha))}{r_3^2 - r_2^2}, \\
N_3 &= \frac{r_2 r_3 (r_3 \sin(\varphi_1 - \alpha) + r_2 \sin \theta_{12})}{r_3^2 - r_2^2}.
\end{aligned}
\right\}
\tag{3.3}
$$

It is noteworthy that an interface with $N = 0$ assumes a shape of spherical cap, and consequently, the radius of the spherical cap is $2/M$. Thus, among the interfaces in configuration C, either I_{12} or I_{23} does not assume a spherical shape, but I_{13} does. To simplify the computation of M and N, we consider the balance between the Laplace pressures

$$
M_1 \sigma_{23} - M_2 \sigma_{13} + M_3 \sigma_{12} = p_2 - p_3 - (p_1 - p_3) + (p_1 - p_2) = 0.
\tag{3.4}
$$

In the expressions (3.1)–(3.3), there are four unknowns: α; r_1; r_2; and r_3. In addition to the three constraints, i.e. the volumes of droplets 1 and 2, and the force balance (3.4), it is necessary to have one more constraint to uniquely determine the four unknowns. Here, the additional constraint is a geometrical one, i.e. I_{12} and I_{23} have the same height, which can be expressed as

$$
\left| \int_{r_1}^{r_2} \tan \phi_1 \, dx_1 \right| = \left| \int_{r_3}^{r_2} \tan \phi_3 \, dx_3 \right|.
\tag{3.5}
$$

To get α, r_1, r_2 and r_3, a shooting method is used to find the solutions that satisfy the constraints, along with a fourth-order Runge–Kutta scheme to approximate the integration.
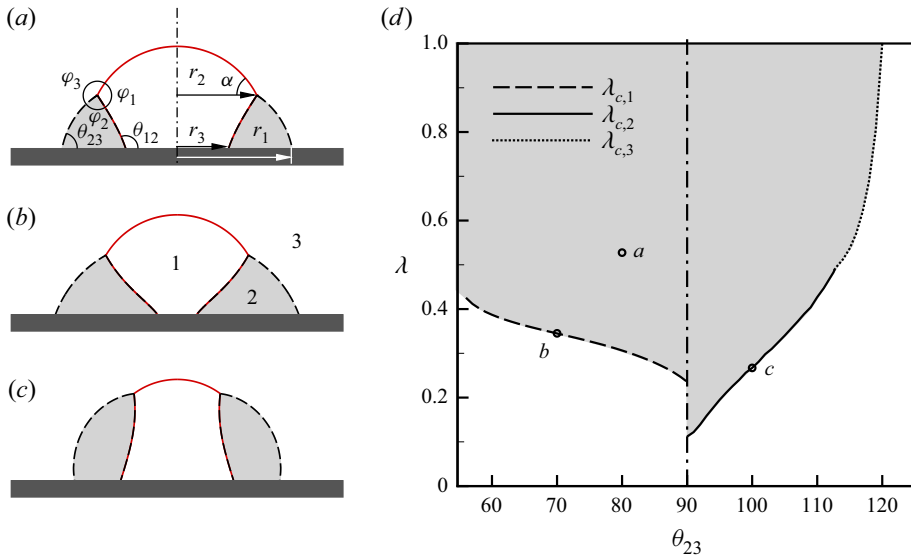
Figure 3. Geometry and configuration boundaries of configuration C. Panel (a) shows the general drop shape of configuration C with $\theta_{23} = 80°$ and $\lambda = 0.500$. The drop shapes at the critical conditions are shown in panel (b) $\theta_{23} = 70°$ and $\lambda = 0.341$ and panel (c) $\theta_{23} = 100°$ and $\lambda = 0.267$). Panel (d) shows the regime diagram with respect to λ and θ_{23}, in which the grey indicates the region where the configuration C is stable. The boundaries are represented by three critical volume ratios: $\lambda_{c,1}$ (at which r_3 reaches a minimum value below which there is no solution for configuration C), $\lambda_{c,2}$ (at which r_2 reaches a minimum value) and $\lambda_{c,3}$ (at which $r_1 = r_3$).

The phase boundaries of configuration C heavily relies on the value of θ_{23}. We note that θ_{23} and θ_{21} ($= 180° - \theta_{12}$) are similar, in the sense that they both are acute angles (see e.g. figure 3b) or obtuse angles (see e.g. figure 3c) at the same time according to (2.3). It is natural to expect from a geometrical point of view that configuration transition would not occur unless the contact line of I_{12} moves inwards and meets at the z-axis for $\theta_{23} < 90°$, i.e. $r_3 = 0$; similarly, it is expected for $\theta_{23} > 90°$ that either the vanishing of I_{13} (i.e. $r_2 = 0$) or the merging of the contact lines of I_{23} and I_{12} on the substrate (i.e. $r_1 = r_3$) could lead to the occurrence of configuration transition. However, our theoretical solutions suggest that these geometrical conditions do not correspond to the transition boundaries of configuration C.

Figure 4(a) shows the solution at $\theta_{23} = 70°$ in terms of r_3 versus λ. Firstly, we can see that there exists a minimum value of r_3, i.e. $r_{3,min} = 0.233$ at $\lambda_{c,1} = 0.345$, below which there is no solution for configuration C. In other words, configuration transition for $\theta_{23} < 90°$ occurs much earlier than the prediction of geometrical condition, i.e. $r_3 = 0$. Secondly, we observe that configuration C might have multiple solutions with the same parameters. For example, there are two solutions of compound sessile drops in the configuration C at $\lambda = 0.6$: $r_3 = 0.601$ and $r_3 = 0.030$, of which the drop shapes are shown in figures 4(b) and 4(d), respectively. Our numerical simulation indicates that an initial set-up of a drop with $r_3 = 0.030$ is unstable and gradually transits to the equilibrium state with $r_3 = 0.601$ (figure 4e). The variation of the rescaled surface energy E_S with $\theta_{23} = 70°$ is also shown in figure 4(a). We can see that the surface energy of the drop shape in figure 4(d) is higher than that of figure 4(b), and the lowest surface energy occurs at $r_3 = r_{3,min}$. In fact, the theoretical prediction of configuration C at $\theta_{23} = 70°$ is a saddle-point bifurcation, and has two branches of solutions – see figures 4(a). The turning point ($r_3 = r_{3,min}$ and
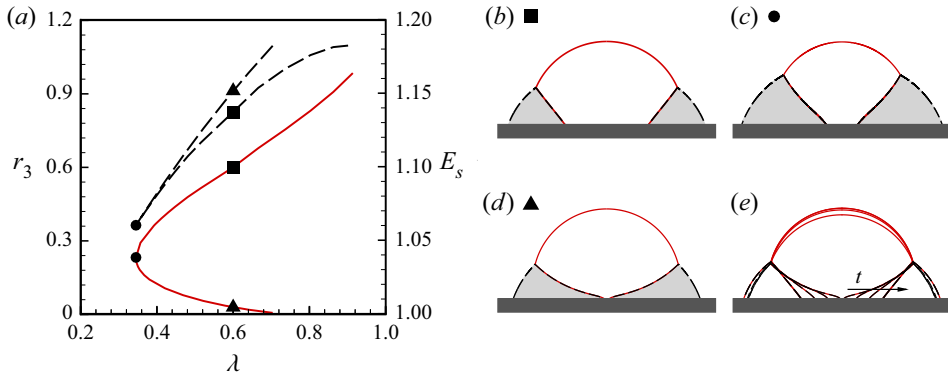
Figure 4. Saddle-point bifurcation in the solution of configuration *C*. (*a*) Contact line position r_3 (solid lines) and the rescaled system energy E_S (dashed lines) at $\theta_{23} = 70°$ as a function of volume ratio λ. (*b*) One theoretical prediction of the drop geometry with $\lambda = 0.600$ and $r_3 = 0.601$ (denoted by ■ in panel (*a*)). (*c*) The drop geometry at the onset of configuration transition at $\lambda = 0.345$ and $r_3 = 0.233$ (denoted by ● in panel (*a*)). (*d*) The non-physical theoretical prediction of the drop geometry with $\lambda = 0.600$ and $r_3 = 0.601$ (denoted by ▲ in panel (*a*)). (*e*) Temporal evolution of the drop geometry from panel (*d*) to panel (*b*) obtained by numerical simulations. The arrow indicates the sequence of the times.

$\lambda_{c,1} = 0.345$) separating the unstable solutions (the lower branch) from the stable ones (the upper branch) also represents the phase boundary at $\theta_{23} = 70°$. In other words, the saddle-point bifurcation represents another type of criteria for the onset of configuration transition, in addition to the geometrical criteria. In such a way, we can theoretically predict the phase boundary of configuration *C* at $\theta_{23} < 90°$, which is included in figure 3(*d*).

Also due to the occurrence of the saddle-point bifurcation, the geometrical condition $r_2 = 0$ for $\theta_{23} > 90°$ underestimates the value of r_2 at onset of configuration transition. The solution of the phase boundary is plotted in terms of $\lambda_{c,2}$ versus θ_{23} in figure 3(*d*). In addition, the third critical condition for configuration *C*, i.e. $r_1 = r_3$, has effects on the configuration transition for $\theta_{23} > 90°$ too (denoted by $\lambda_{c,3}$ versus θ_{23} in figure 3*d*), thereby leading to the phase boundary in this range of θ_{23} consisting of two curves.

The effect of changing interface tension coefficients on the phase boundaries can also be qualitatively analysed here. The change of any interface tension coefficient among σ_{12}, σ_{13} and σ_{23} would result in the variation of the interface angles and the interface curvatures M (see also (3.4)), thereby causing the position change of the triple-phase line. Therefore, we can expect that the phase boundaries would be changed accordingly, but the pattern should be similar. For example, around $\theta_{23} = 90°$, the phase boundaries are represented by $\lambda_{c,1}$ (for $\theta_{23} < 90°$) and $\lambda_{c,2}$ (for $\theta_{23} > 90°$), respectively. The slope of I_{12} accounts for this sharp change in the phase boundaries, in the sense that it determines which would firstly intersect with the axis of symmetry: the moving contact line or the triple-phase point. As a result, a sharp change in the phase boundaries always occurs at $\theta_{12} = 90°$ (or equivalently, $\theta_{23} = 90°$ according to (2.3)), regardless of the variation of interface tension coefficients.

3.2. *Encapsulation*

A typical compound sessile drop with configuration *E* is showed in figure 5(*a*). The compound sessile drop has two interfaces, i.e. I_{12} and I_{23}, characterized by the radius of the wetted area, i.e. r_3 and r_1, respectively. Therefore, the boundary conditions are: $\phi|_{x=r_3} = \theta_{12}$ at the contact line and $\phi|_{x=0} = 0$ at the symmetry axis for I_{12}; and $\phi|_{x=r_1} = \theta_{23}$ at the contact line and $\phi|_{x=0} = 0$ at the symmetry axis for I_{23}. The interface shapes at
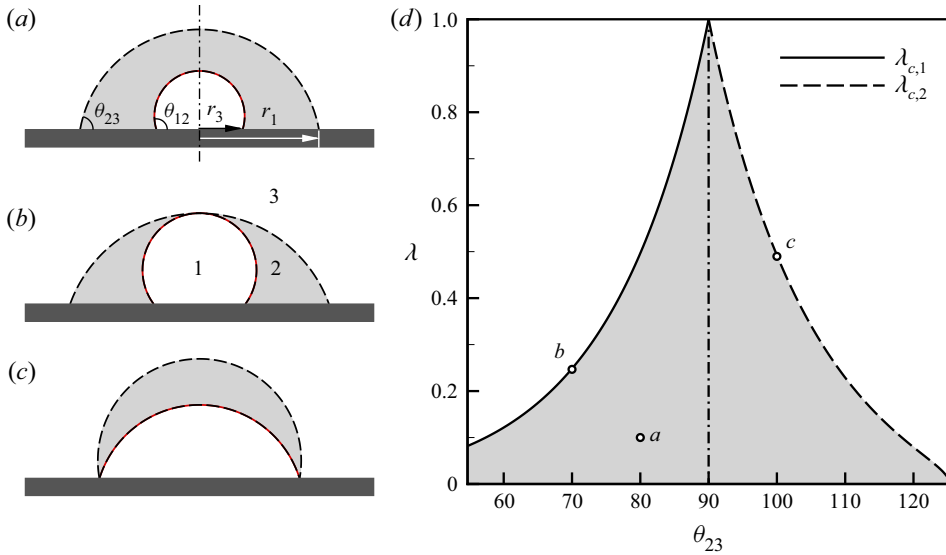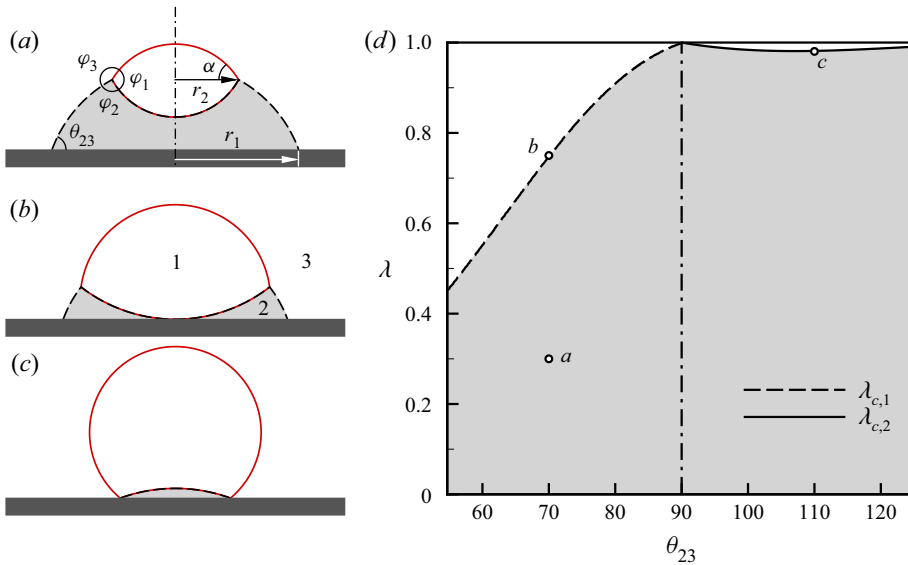
917 A37-9

Figure 5. Geometry and configuration boundaries of configuration E. Panel (a) shows the drop geometry with $\theta_{23} = 80°$ and $\lambda = 0.100$, panels (b,c) represent the geometrical criteria for the occurrence of configuration transition, and panel (d) shows the regime diagram with respect to λ and θ_{23}, in which the grey indicates the region where the configuration E is stable. The boundaries correspond to the two critical volume ratios: $\lambda_{c,1}$ (solid line) and $\lambda_{c,2}$ (dashed line), respectively.

equilibrium can be solved by taking these boundary conditions into account. Specifically, we can get $(M_3, N_3) = (2 \sin \theta_{12}/r_3, 0)$ and $(M_1, N_1) = (2 \sin \theta_{23}/r_1, 0)$. Thus, both I_{12} and I_{23} are spherical caps. From the calculation of drop volume, it is easy to associate r_3 and r_1 with λ and contact angles

$$\frac{r_3}{R} = \sqrt[3]{\frac{4\lambda}{V(\theta_{12})}} \quad \text{and} \quad \frac{r_1}{R} = \sqrt[3]{\frac{4}{V(\theta_{23})}}, \qquad (3.6a,b)$$

where the function V is defined as $V(\xi) = (1 - \cos \xi)^2 (2 + \cos \xi)/\sin^3 \xi$.

With the variation of λ and/or θ_{23}, the two interfaces may come into contact – see e.g. figures 5(b) and 5(c). Occurrence of configuration transition can be expected in these cases, thereby defining the phase boundary of configuration E. The contact of the interfaces would occur at the top of the drop when $\theta_{23} < \theta_{12}$ (figure 5b), or at the contact line when $\theta_{23} > \theta_{12}$ (figure 5c). Mathematically, the phase boundaries can be expressed as $r_3(1 - \cos \theta_{12})/\sin \theta_{12} = r_1(1 - \cos \theta_{23})/\sin \theta_{23}$ in the former, and $r_1 = r_3$ in the latter, which is consistent with the work of Mahadevan *et al.* (2002). Accordingly, the two phase boundaries can be described with respect to the critical volume ratio, $\lambda_{c,1}$ and $\lambda_{c,2}$, as a function of the contact angles, by substituting (3.6a,b) into these two conditions. That is,

$$\lambda_{c,1} = \frac{(1 - \cos \theta_{23})(2 + \cos \theta_{12})}{(1 - \cos \theta_{12})(2 + \cos \theta_{23})} \quad \text{and} \quad \lambda_{c,2} = \frac{V(\theta_{12})}{V(\theta_{23})}. \qquad (3.7a,b)$$

The two boundaries in (3.7a,b) are plotted in figure 5(d) to define the phase diagram of configuration E with respect to λ versus θ_{23}, of which the result is similar to that of a hollow sessile drop (Gao & Feng 2011). Because of $\cos \theta_{12} = -\sqrt{3} \cos \theta_{23}$ in the present study, we can get $\lambda_{c,1} = \lambda_{c,2} = 1$ at $\theta_{23} = 90°$, which corresponds to $\theta_{23} = \theta_{12}$. This implies that the configuration E is always stable at $\theta_{23} = 90°$, since the two interfaces

917 A37-10

Figure 6. Geometry and configuration boundaries of configuration L. Panel (a) shows the drop geometry with $\theta_{23} = 70°$, $\lambda = 0.300$, panels (b,c) represent the geometrical criteria for the occurrence of configuration transition at ($\theta_{23} = 70°$, $\lambda = 0.747$) and ($\theta_{23} = 110°$, $\lambda = 0.982$), respectively, and panel (d) shows the regime diagram with respect to λ and θ_{23}, in which the grey indicates the region where the configuration L is stable. The boundaries correspond to the two critical volume ratios: $\lambda_{c,1}$ (solid line) and $\lambda_{c,2}$ (dashed line), respectively.

are concentrically spherical caps in this case. Furthermore, because the only two interfaces (I_{12} and I_{23}) do not come into contact until the occurrence of configuration transition, the variation of interfacial tension coefficients has no effect on the phase boundaries of configuration E (represented by $\lambda_{c,1}$ and $\lambda_{c,2}$) if the contact angles are fixed.

3.3. *Lens*

Figure 6(a) shows a typical compound sessile drop with configuration L, of which only I_{23} is in contact with the substrate, with the radius of the wetted area denoted by r_1. The triple-phase line, where three interfaces of the compound drop meet, is also the boundary point shared among the interfaces. Defining the position of the triple-phase line as (r_2, α) and taking $\phi|_{x=0} = 0$ at the symmetry axis into account, we can get $(M_2, N_2) = (2\sin\alpha/r_2, 0)$. Similarly, the boundary conditions for I_{12} can be obtained: $\phi|_{x=r_2} = 180° - \varphi_1 + \alpha$ (from geometrical relation at the triple-phase line) and $\phi|_{x=0} = 180°$, leading to the solution of $(M_3, N_3) = (2\sin(\varphi_1 - \alpha)/r_2, 0)$. Therefore, the interfaces I_{13} and I_{12} are both spherical caps as $N_2 = N_3 = 0$. This fact allows us to relate r_2 with λ, φ_1 and α through the volume formula for a spherical cap

$$\frac{r_2}{R} = \sqrt[3]{\frac{4\lambda}{V(\alpha) + V(\varphi_1 - \alpha)}}. \tag{3.8}$$

For I_{23}, the boundary conditions are $\phi|_{x=r_1} = \theta_{23}$ at the contact line and $\phi|_{x=r_2} = \varphi_3 + \alpha - 180°$ at the triple-phase point. Taking account of the balance between the Laplace pressures (3.4), we can get $(M_1, N_1) = (2\sin\theta_{23}/r_1, 0)$ and the radius ratio of r_1 to r_2,

$$\eta = \frac{r_1}{r_2} = \frac{-\sin\theta_{23}}{\sin(\alpha + \varphi_3)}. \tag{3.9}$$

Figure 7. Superimposed phase diagrams of configurations *L*, *E* and *C* with respect λ to θ_{23}.

relative position illustrated in figure 1(*a–c*), and thus those cases in which fluid 1 switches the position with fluid 2 are not included.

On the other hand, one may ask what configuration a compound sessile drop would be for specific parameters. To answer this question, it is necessary to know the initial configuration of the drop and the route of parameter change to the specific parameters, which affect the evolution history of geometry and energy of the drop and consequently determine its final state. In the following, we investigate the configuration transitions by a combination of surface energy analysis and numerical simulations.

4.2. *History dependence of configuration transition*

To show the effect of initial configuration of the drop and the route of parameter change on the configuration transition, we investigate the variation of E_S as a function of λ, for a fixed value of θ_{23} (= 80°). The theoretical prediction of E_S as a function of λ is shown in figure 8(*i*). At low λ (= 0.1), two types of compound sessile drops can exist stably, in the configurations *E* (figure 8*a*) and *L* (figure 8*b*), respectively. If a compound drop takes the configuration in figure 8(*a*) as its initial configuration, E_S increases monotonically with λ until a configuration transition occurs (i.e. at $\lambda = 0.497$, which corresponds to the boundary between the zones *V* and *VI*). More precisely, the inside droplet of fluid 1 becomes so big that it starts to touch the interface I_{23} (figure 8*e*), thereby leading to the generation of a new interface, i.e. I_{13}. We simulate the dynamic process of this configuration transition at $\lambda = 0.497$, and show the results in figure 9(*a*), with respect to the snapshots of the drop at different times. It can be seen that after the generation of I_{13}, the contact line of I_{12} moves inwards, and the compound sessile drop gradually evolves into an equilibrium state in configuration *C*, of which the shape is well predicted by the theoretical analysis (figure 8*f*).

The transition process from the state in figure 8(*e*) to that in figure 8(*f*) is also accompanied by the dissipation of surface energy (figure 8*i*). As a result, if we reverse the manipulation of λ now, i.e. reducing it from 0.497 to 0.1, it is expected that the compound sessile drop will not return to its initial state (figure 8*a*), but to the state in
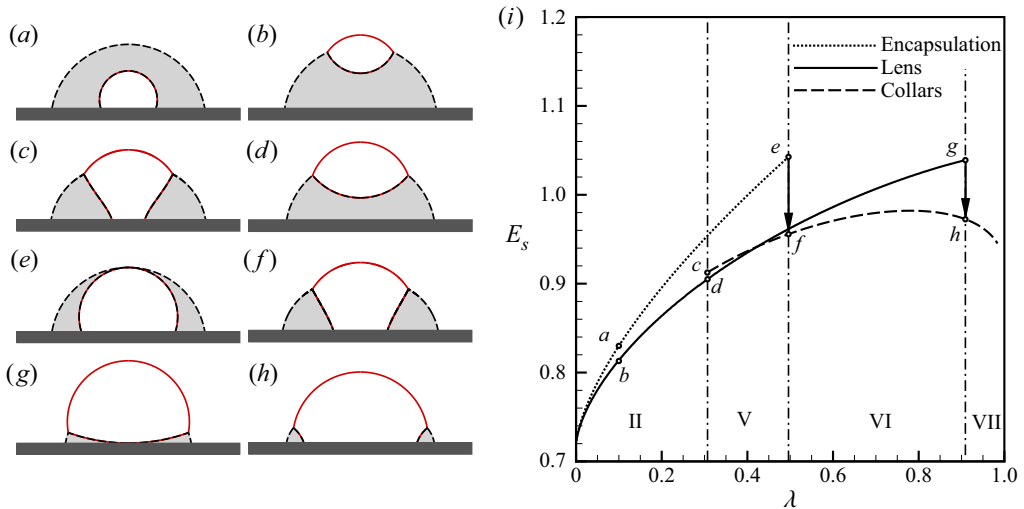
Figure 8. Geometry of compound sessile drops and transition among the three configurations at $\theta_{23} = 80°$. (*a,b*) Configurations *E* and *L* at $\lambda = 0.100$, respectively; (*c,d*) configurations *C* and *L* at $\lambda = 0.307$, respectively; (*e,f*) configurations *E* and *L* at $\lambda = 0.497$, respectively; (*g,h*) configurations *L* and *C* at $\lambda = 0.911$, respectively; (*i*) surface energy E_S as a function of λ.
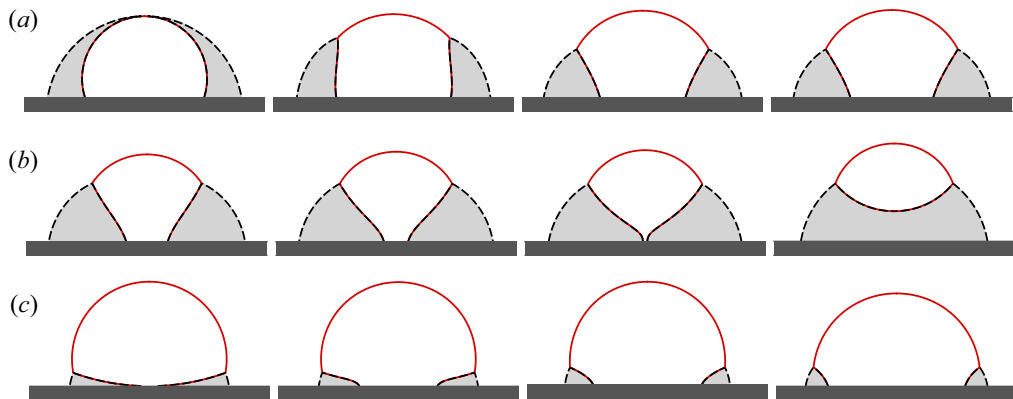

Figure 9. Snapshots of configuration transition at $\theta_{23} = 80°$: (*a*) from *E* to *C* at the boundary between zone *V* and *VI* ($\lambda = 0.497$) at times $t = 0, 1, 2, 10$ (from left to right); (*b*) from *L* to *C* at the boundary between zone *VI* and *VII* ($\lambda = 0.911$) at times $t = 0, 1, 5, 20$; and (*c*) from *C* to *L* at the boundary between zone *V* and *II* ($\lambda = 0.307$) at times $t = 0, 5, 12.8, 30$.

configuration *L* shown in figure 8(*b*). It is also noteworthy that in this reverse manipulation of λ, another configuration transition would occur at $\lambda = 0.307$, which corresponds to the boundary between zones *II* and *V*. Accordingly, the compound sessile drop will change from configuration *C* (figure 8*c*) to configuration *L* (figure 8*d*), which has also been confirmed by numerical simulations – the transition dynamics can be seen in figure 9(*b*).

It is crucial in practice to know how to control the configuration transition. One can get some clues from figure 8 to the route design of parameter variation. First, at $\theta_{23} = 80°$, configuration *E* always has the highest surface energy level among the three configurations, e.g. in the zones *II* and *V* where it exists. Therefore, it is reasonable to expect that the transition from the other two configurations to configuration *E* cannot be

achieved by simply varying λ. Second, we find that the surface energy of configuration L catches up with that of configuration C in the zone V with increasing λ, resulting in the intersection of their surface-energy curves (figure 8i). This suggests that we can control the configuration of a compound sessile drop in the zones V and VI (to be either configuration C or configuration L) by varying λ, regardless of its initial shape. For example, to make a compound drop initially with configuration L transit to configuration C with the same λ, one can increase λ to the critical value $\lambda = 0.911$ (at the boundary between the zones VII and VI), at which configuration transition from L to C occurs (see figure 9c for the dynamic process from numerical simulations), and then decrease λ to the initial value. To reverse the configuration transition, one can decrease λ to 0.307, i.e. the boundary between the zones II and V, so that the compound drop transits from configuration C to L – after then, increasing λ to the initial value would complete the task. Such transitions between configurations L and C can be continued, so that the graph of E_S versus λ appears to form a complete circle among the four states of d, g, h and c in figure 8(i), namely, a butterfly loop. Obviously, the presence of the butterfly loop facilitates the control of the configuration transition in practice.

4.3. *Dynamics of configuration transition*

We investigate the dynamics of configuration transition by numerical simulations, and reveal some interesting phenomena that are not accessible to theoretical analysis. Figure 10 shows two cases of transition to configuration L. In the first case ($\theta_{23} = 70°$ and $\lambda = 0.248$), I_{12} contacts with I_{23} at the apex of the drop, thereby leading to the generation of a new interface and an apparent configuration transition from E to C; however, the contact line of I_{12} contracts inwards continuously, eventually resulting in the detachment of I_{12} from the wall and the configuration transition from C to L (figure 10a). In the second case ($\theta_{23} = 110°$ and $\lambda = 0.360$), the dynamic process of the transition seems to proceed the opposite way around compared with the first case, but also ends up with configuration L. We can see in figure 10(b) that the shrinkage of I_{13} causes the encapsulation of an inside droplet, i.e. the occurrence of transition from configuration C to E; after then, continuous spreading of the contact line of I_{12} makes the interfaces I_{23} and I_{12} meet on the wall, leading to the reappearance of I_{13} at the wall and the subsequent transition from configuration E to L. Furthermore, during the shrinkage of I_{13}, a small droplet is pinched off from droplet 1 by the induced capillary waves and floats at the apex of the compound drop. The drop pinch off is primarily due to the inertial effect of I_{12}, which would be suppressed if a larger Oh number is used ($Oh = 0.1$ in the present study). Despite the difference in transition dynamics between the two cases, they have one thing in common, i.e. the transition passes through an intermediate unstable state to reach the configuration at equilibrium.

Numerical simulations also indicate that configuration transition might not proceed as predicted by the phase diagram in figure 7, in particular when θ_{23} is an obtuse angle. Figure 11 shows two such examples. Snapshots of configuration transition from E to L with $\theta_{23} = 110°$ and $\lambda = 0.229$ are shown in figure 11(a). In this case, the volume ratio of the internal droplet in configuration E reaches the boundary between the zones II and III; according to the phase diagram in figure 7, the compound drop would transit to configuration L, and end up with an equilibrium shape as shown in figure 11(c). Numerical results indicate that the transition to configuration L has been achieved, but compared with the theoretical prediction, the drop shape at equilibrium is upside down with respect to the relative position of droplets 1 and 2. This is primarily due to the fact that we do not consider the cases in which fluid 1 switches the position with fluid 2 in figure 7, and that
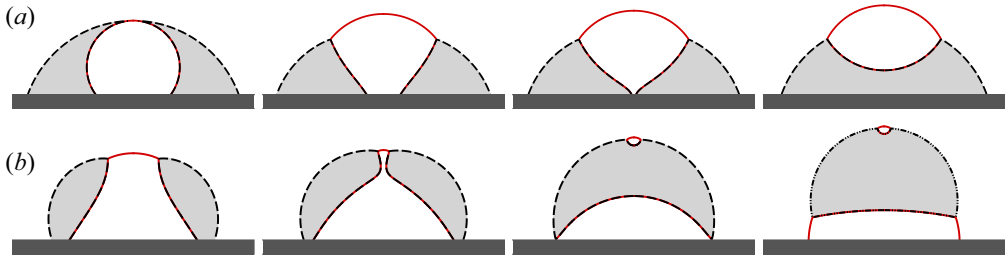
Figure 10. Dynamic process of morphological transformation. (*a*) Snapshots of configuration transitions at the boundary between the zones *I* and *II* (specifically, $\theta_{23} = 70°$ and $\lambda = 0.248$) at times $t = 0$, 4, 6.8, 20 (from left to right). (*b*) Snapshots of configuration transition from *C* to *L* with $\theta_{23} = 110°$ and $\lambda = 0.360$, at times $t = 0$, 2.6, 5, 10. Note that in these cases the transition passes through an intermediate unstable state to reach the configuration at equilibrium.
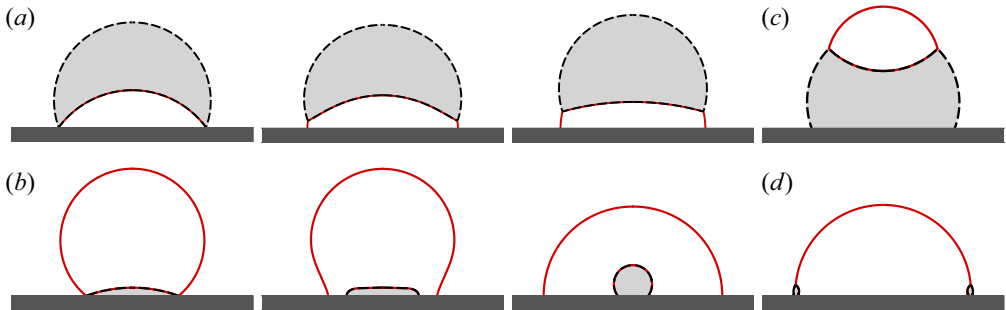

Figure 11. Dynamic process of morphological transformation. (*a*) Snapshots of configuration transition from *E* to *L* at the boundary between the zones *II* and *III* boundary (with $\theta_{23} = 110°$ and $\lambda = 0.229$) at the times $t = 0$, 1, 10 (from left to right). (*b*) Snapshots of configuration transition from *L* to *E* at the boundary between the zones *IV* and *VIII* (with $\theta_{23} = 110°$ and $\lambda = 0.982$) at times $t = 0$, 0.2, 10 (from left to right). Note that the relative positions of fluid 1 and fluid 2 in the last panels of (*a*,*b*) are reversed as compared with the regular configurations in figure 1. Panels (*c*,*d*) show the results of configuration transition as predicted by the phase diagram in figure 7, with the same initial conditions as in panel (*a*) and panel (*b*), respectively.

the configuration *L* with the position of droplets 1 and 2 being switched is also stable for this set of parameters. Figure 11(*b*) shows a similar case of configuration transition at the boundary between the zones *IV* and *VIII* (with $\theta_{23} = 110°$ and $\lambda = 0.982$), in which the droplet 1 engulfs the droplet 2 during the transition. Consequently, the compound drop eventually falls into the configuration *E*, rather than the configuration *C* (as shown in figure 11*d*) predicted by the phase diagram. These suggest that the reversal of fluid position in a compound sessile drop can be manipulated through configuration transition.

We can take account of the configuration *L* in which fluid 1 is in contact with the substrate and droplet 2 sits on droplet 1, simply by replacing θ_{23} with θ_{13} in the theoretical analysis. In such a way, we can obtain the theoretical prediction of the phase boundary for this particular configuration *L*. Note that θ_{13} is fixed to $90°$ in the present study, and thus the phase boundary is only a function of λ. Specifically, the configuration *L* is stable for $\lambda > 0.0792$ in this case, which is consistent with the observation in figure 11(*a*). Furthermore, configuration transitions similar to figure 11(*b*) would be expected for $\lambda \leq 0.0792$.

917 A37-16

5. Conclusion

We have investigated the configuration boundaries and transitions of compound sessile drops by theoretical analysis and numerical simulations, in particular for the configurations encapsulation, lens and collars, respectively. The investigations were performed in the parameter space of the wettability of the substrate θ_{23} and the volume ratio of the two component droplets λ, and more specifically, $\lambda \in [0, 1]$ and $\theta_{23} \in [55°, 125°]$. We revealed that there are two types of criteria for the onset of transition among the configurations. One is related to the critical conditions of drop geometry, including the contact between the interfaces and the merging of the contact lines; the other corresponds to the minimum of the surface energy when the interface solution has a saddle-point bifurcation (e.g. collars configuration). Based on these criteria, we established the boundaries for each configuration in the parameter space. We found that the configuration transitions are path dependent, and moreover, identified the irreversible and reversible configuration transitions. In particular, the graph of E_S versus λ for the reversible configuration transitions appears to form a butterfly loop. This finding provides a way of designing the variation of physical parameters, so as to facilitate the reconfiguration of the compound sessile drops. The dynamic behaviours were studied by numerical simulations, and it was found that the transition might pass through an intermediate, unstable configuration before reaching the final stable one.

In the present study, we only consider the configuration transition due to the variation of λ and θ_{23}. In principle, the configuration transition can also result from the variation of interface tensions, e.g. using surfactants as in the experiments (Li *et al.* 2020*b*) to control the morphological configuration for sessile drops.

Declaration of interests. The authors report no conflict of interest.

Author ORCIDs.
Peng Gao https://orcid.org/0000-0002-1003-3370;
Er-Qiang Li https://orcid.org/0000-0002-5003-0756;
Hang Ding https://orcid.org/0000-0002-7395-6332.

Appendix A. Computation of surface energy for compound sessile drops at equilibrium

The surface energy of a compound sessile drop is a function of its interface areas and interface tension coefficients. For a single droplet on the substrate with the contact angle ξ and the radius of wetting area r, the droplet volume can be simply calculated by $V(\xi) = (1 - \cos \xi)^2 (2 + \cos \xi)/ \sin^3 \xi$, and the area of the droplet surface is $S_c = 2\pi r^2 (1 - \cos \xi)/ \sin^2 \xi$.

A.1. *Surface energy of configuration E*

For configuration E, both I_{23} and I_{12} are spherical caps. Defining the surface area of I_{23} and I_{12} as S_{23} and S_{12}, respectively, we can easily have $S_{23} = 2\pi r_1^2 (1 - \cos \theta_{23})/ \sin^2 \theta_{23}$ and $S_{12} = 2\pi r_3^2 (1 - \cos \theta_{12})/ \sin^2 \theta_{12}$. Therefore, the surface energy of system yields

$$E = S_{12}\sigma_{12} + S_{23}\sigma_{23} + \pi r_3^2 \sigma_{1s} + \pi(r_1^2 - r_3^2)\sigma_{2s} + (S_0 - \pi r_1^2)\sigma_{3s}, \qquad (A1)$$

917 A37-17

where σ_{is} denotes the interface tension between the fluid i and the substrate, and S_0 is the total area of substrate. Taking account of $\sigma_{ij} \cos \theta_{ij} = \sigma_{js} - \sigma_{is}$, for $i, j = 1, 2, 3$, (A1) can be rewritten as

$$E = (S_{12} - \pi r_3^2 \cos \theta_{12})\sigma_{12} + (S_{23} - \pi r_1^2 \cos \theta_{23})\sigma_{23} + S_0\sigma_{3s}. \tag{A2}$$

Because S_0 and σ_{3s} are constants, the surface energy of the system can be generally rescaled as $E_S = (E - S_0\sigma_{3s})/(4\pi R^2 \sigma_{13})$. Consequently, the rescaled surface energy or configuration E gives

$$E_S = \frac{1}{4\pi R^2 \sin \varphi_2}((S_{12} - \pi r_3^2 \cos \theta_{12}) \sin \varphi_3 + (S_{23} - \pi r_1^2 \cos \theta_{23}) \sin \varphi_1). \tag{A3}$$

A.2. *Surface energy of configuration L*

Similarly for configuration L, the area of three interfaces can be expressed as: $S_{12} = 2\pi r_2^2(1 + \cos(\varphi_1 - \alpha))/\sin^2(\varphi_1 - \alpha)$; $S_{23} = 2\pi r_1^2/(1 - \cos \theta_{23})/\sin^2 \theta_{23} - 2\pi r_2^2(1 - \cos(\pi - \varphi_2 - \varphi_1 + \alpha))/\sin(\pi - \varphi_2 - \varphi_1 + \alpha)$; and $S_{13} = 2\pi r_2^2(1 - \cos \alpha)/\sin^2 \alpha$. Therefore, the rescaled surface energy E_S can be calculated by

$$E_S = \frac{1}{4\pi R^2 \sin \varphi_2}(S_{13} \sin \varphi_2 + S_{12} \sin \varphi_3 + (S_{23} - \pi r_1^2 \cos \theta_{23}) \sin \varphi_1). \tag{A4}$$

A.3. *Surface energy of configuration C*

In configuration C, I_{13} is the only spherical cap. Its surface area and volume are calculated by $S_{13} = 2\pi r_3^2(1 - \cos \alpha)/\sin^2 \alpha$ and $V_{13} = \pi r_3^3 V(\alpha)/3$, respectively. Because I_{12} and I_{23} are not spherical caps, their surface areas (S_{12} and S_{23}) and volumes (V_{12} and V_{23}) need to be calculated by numerical integration. Then, the rescaled surface energy E_S is calculated by

$$E_S = \frac{1}{4\pi R^2 \sin \varphi_2}(S_{13} \sin \varphi_2 + (S_{12} - \pi r_3^2 \cos \theta_{12}) \sin \varphi_3 + (S_{23} - \pi r_1^2 \cos \theta_{23}) \sin \varphi_1). \tag{A5}$$

REFERENCES

BANSAL, S. & SEN, P. 2017 Axisymmetric and nonaxisymmetric oscillations of sessile compound droplets in an open digital microfluidic platform. *Langmuir* **33** (41), 11047–11058.

CARROLL, B.J. 1976 The accurate measurement of contact angle, phase contact areas, drop volume, and laplace excess pressure in drop-on-fiber systems. *J. Colloid Interface Sci.* **33** (3), 488–495.

GAO, P. & FENG, J.J. 2011 Spreading and breakup of a compound drop on a partially wetting substrate. *J. Fluid Mech.* **682**, 415–433.

IQBAL, S., DHIMAN, S., SEN, A.K. & SHEN, A.Q. 2017 Dynamics of a water droplet over a sessile oil droplet: compound droplets satisfying a Neumann condition. *Langmuir* **33** (23), 5713–5723.

KELLER, K., YAKOVLEV, A.V., GRACHOVA, E.V. & VINOGRADOV, A.V. 2018 Inkjet printing of multicolor daylight visible opal holography. *Adv. Funct. Mater.* **28** (21), 1706903.

LI, D., DEL HIERRO, G.R., DI, J.Z. & ZUO, Y.Y. 2020a Compound drop shape analysis with the Neumann number. *Langmuir* **36** (26), 7619–7626.

LI, Y., DIDDENS, C., SEGERS, T., WIJSHOFF, H., VERSLUIS, M. & LOHSE, D. 2020b Evaporating droplets on oil-wetted surfaces: suppression of the coffee-stain effect. *Proc. Natl Acad. Sci. USA* **117**, 16756–16763.

LIU, H.R. & DING, H. 2015 A diffuse-interface immersed-boundary method for two-dimensional simulation of flows with moving contact lines on curved substrates. *J. Comput. Phys.* **294**, 484–502.

MAHADEVAN, L., ASSA-BEDIA, M. & POMEAU, Y. 2002 Four-phase merging in sessile compound drops. *J. Fluid Mech.* **451**, 411–420.

NEESON, M.J., TABOR, R.F., GRIESER, F., DAGASTINE, R.R. & CHAN, D.Y.C. 2012 Compound sessile drops. *Soft Matt.* **8**, 11042–11050.

SUNDARARAJAN, P., WANG, J., ROSEN, L.A., PROCOPIO, A. & ROSENBERG, K. 2017 Engineering polymeric janus particles for drug delivery using microfluidic solvent dissolution approach. *Chem. Engng Sci.* **178**, 199–210.

ZARZAR, L.D., SRESHT, V., SLETTEN, E.M., KALOW, J.A., BLANSCHTEIN, D. & SWAGER, T.M. 2015 Dynamically reconfigurable complex emulsions via tunable interfacial tensions. *Nature* **518**, 520–524.

ZHANG, C.Y., DING, H., GAO, P. & WU, Y.L. 2016 Diffuse interface simulation of ternary fluids in contact with solid. *J. Comput. Phys.* **309**, 37–51.